Photonic Frequency Down Conversion Approach to Measure Microwave Signal Angle of Arrival

Chongjia Huang and Erwin Hoi Wing Chan, *Senior Member, IEEE*

***Abstract*—This paper presents an angle-of-arrival (AOA) measurement system based on microwave photonic frequency down conversion. It has the novelty of no LO is needed for the frequency conversion process. Instead, a ramp waveform is used to shift the frequency of an optical carrier, which is phase modulated by a microwave signal in the subsequent stage. Two low-frequency IF signals are generated after photodetection. The AOA of the incoming microwave signal can be determined by measuring the phase difference of the two IF signals. Comparing with the previously reported frequency converter based AOA measurement systems, the proposed structure does not need a high-frequency tunable LO source and high-frequency electrical components. Expensive and bulky equipment such as an electrical spectrum analyser are not required in the proposed AOA measurement system. Experimental results show AOA measurement of different-frequency and different-power microwave signals, with small measurement errors.**

***Index Terms*—Angle of arrival, direction finding, frequency down conversion, frequency shifter, microwave photonics.**

I. Introduction

IT IS of interest to use microwave photonic techniques to obtain various microwave signal parameters such as the amplitude, phase and frequency of a microwave signal. This arises from the broadband, high-speed and high-resolution capabilities of microwave photonics [1]. The phase difference of a microwave signal received by two antennas can be used to determine the microwave signal angle-of-arrival (AOA), which has numerous applications in position systems, communication systems and electronic warfare systems [2]–[4].

Various photonic-assisted AOA measurement techniques have been reported in the past 25 years. One approach is to design the system such that the output signal amplitude is dependent on the phase difference of the incoming microwave signal received by two antennas [5]–[8]. Therefore, by using devices such as an optical power meter, an RF power meter or a multimeter to measure the output signal amplitude, the microwave signal phase difference and consequently the microwave signal AOA can be determined. However, the output signal amplitude is also affected by the power of the incoming microwave signal. Hence a calibration procedure is needed or the power of the microwave signal into the system needs to be measured prior to AOA measurement. Another AOA measurement approach is based on using a fibre optic delay line filter to produce notches in the system output electrical spectrum [9], [10]. The notch frequency, which is not affected by the power of the incoming microwave signal, can be used to obtain the microwave signal phase difference. However, in this case, the microwave signal AOA measurement range is determined by the microwave signal bandwidth. A broadband microwave signal is needed in order to have a wide AOA measurement range. Furthermore, this approach requires a wideband electrical spectrum analyser (ESA). The AOA of a microwave signal can also be found by using an optical phase scanning technique [11], a wavelength division multiplexing technique [12] and a frequency conversion technique [13]. These techniques enable the microwave signal AOA to be measured without knowing the incoming microwave signal power. However, they are not suitable for use in a long baseline interferometer antenna system [14] because the microwave signal received by two antennas are fed into a single electro-optic modulator, which sets a limit on the antenna separation. Antennas can be placed in different locations in a frequency converter based AOA measurement system [15]. This system is implemented by splitting an LO modulated optical signal into multiple signals, which are launched into a Mach Zehnder modulator (MZM) driven by a microwave signal received by an antenna. Using an electronic phase detector to measure the phase difference of two down converted low-frequency IF signals at photodetector outputs, the microwave signal AOA can be obtained. However, a high-frequency LO source is needed for the frequency conversion process and its frequency needs to be changed with the incoming microwave signal frequency.

The aim of this paper is to present a new frequency converter based AOA measurement system without the need of a high-frequency tunable LO source. The system is designed to down convert the high-frequency incoming microwave signal received by two antennas into two low-frequency IF signals. The IF signals have a phase difference of twice the incoming microwave signal phase difference, which allows the use of a low-frequency electronic phase detector to indirectly acquire the microwave signal phase difference and consequently the microwave signal AOA. Experimental results show the proposed AOA measurement system can measure a $0°-81.5°$ microwave signal AOA with errors less than $\pm 3°$, for 12 to 18 GHz microwave signal and 0.2 to 0.6 modulation indexes.

Manuscript received March 21, 2022; revised April 8, 2022; accepted April 12, 2022. Date of publication April 19, 2022; date of current version May 4, 2022. *(Corresponding author: Erwin Hoi Wing Chan.)*

The authors are with the College of Engineering, IT and Environment, Charles Darwin University, Darwin, NT 0909, Australia (e-mail: 1286660746@qq.com; erwin.chan@cdu.edu.au).

Digital Object Identifier 10.1109/JPHOT.2022.3167987

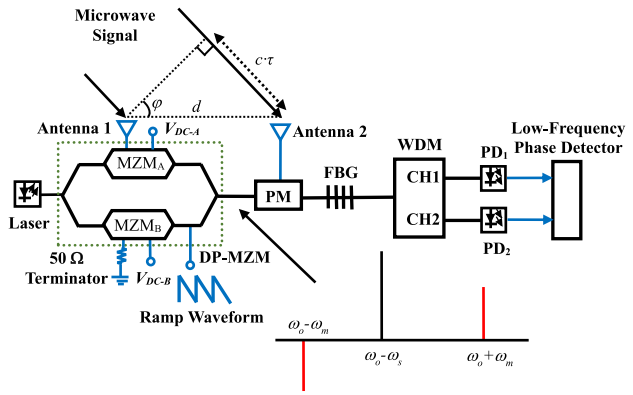

Fig. 1. Frequency converter based AOA measurement system.

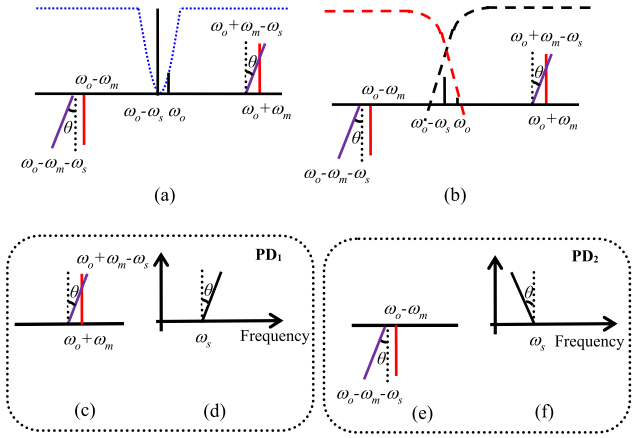

Fig. 2. (a) Phase modulator output spectrum and the FBG reflection spectrum (blue dotted line). (b) FBG output spectrum, and the magnitude response of WDM CH1 (black dashed line) and CH2 (red dashed line). WDM (c) CH1 and (e) CH2 output optical spectrum. (d) PD_1 and (f) PD_2 output electrical spectrum. ω_o, ω_m and ω_s are the angular frequencies of the optical carrier, the incoming microwave signal and the ramp waveform respectively.

II. Structure and Principle of Operation

The proposed photonic-assisted AOA measurement system is depicted in Fig. 1. A laser diode generates a continuous wave light, which has an angular frequency of ω_o. The light is launched into a dual-parallel Mach Zehnder modulator (DP-MZM). The modulator consists of two parallel-connected single-drive MZMs (MZM_A and MZM_B) in a main MZM. Each single-drive MZM has an RF port and a DC port. A microwave signal received by Antenna 1, which has an angular frequency of ω_m, is fed into the RF port of MZM_A. A DC voltage $V_{DC\text{-}A}$ is applied to MZM_A DC port. It is used to set MZM_A bias point at the minimum transmission point (MITP) of the modulator transfer function. As a result, upper and lower microwave signal modulation sidebands at $\omega_o \pm \omega_m$ are generated at MZM_A output. No microwave signal is applied to MZM_B RF port. A DC voltage $V_{DC\text{-}B}$ into MZM_B DC port is set to bias the modulator at the maximum transmission point (MATP). Hence only an optical carrier is present at MZM_B output. A negative slope ramp waveform with an angular frequency ω_s is injected to the DC port of the main MZM. Injecting a signal into the DC port of a MZM can be viewed as injecting a signal into a phase shifter or a low-frequency phase modulator in one arm of a Mach Zehnder interferometer. It has been demonstrated in [16], [17] that the frequency of a light wave can be shifted from f to f-f_s when an optical phase modulator is driven by a ramp waveform with a frequency of f_s and an amplitude of twice the phase modulator half wave voltage. Hence, by designing the ramp waveform amplitude to be twice the main MZM half wave voltage, the angular frequency of the optical carrier at MZM_B output is shifted from ω_o to $\omega_o - \omega_s$. Therefore, the output of the DP-MZM consists of a frequency shifted optical carrier and a pair of microwave signal modulation sideband, as shown in the inset of Fig. 1. The DP-MZM output is connected to a phase modulator (PM), which is driven by the microwave signal received by Antenna 2. As can be seen from Fig. 1, the microwave signal received by Antenna 2 has a time delay τ depending on the microwave signal AOA φ and the two antenna separation d. Hence the microwave signal arrived at Antenna 2 has a phase shift θ compared to the microwave signal arrived at Antenna 1. The microwave signal phase shift is given by

$$\theta = \left(\frac{\omega_m d}{c}\right) \sin\varphi \tag{1}$$

where c is the light speed in vacuum. (1) shows the microwave signal AOA can be determined by measuring the phase shift.

The frequency shifted optical carrier at the angular frequency $\omega_o - \omega_s$ is phase modulated by the microwave signal received by Antenna 2. This generates a pair of microwave signal modulation sidebands at $\omega_o - \omega_s - \omega_m$ and $\omega_o - \omega_s + \omega_m$. The sidebands at the angular frequencies of $\omega_o \pm \omega_m$ into the PM are also modulated by the microwave signal into the PM. This generates a frequency component at the optical carrier frequency ω_o. The optical spectrum after the PM is depicted in Fig. 2(a). The figure reveals that the PM output has two angular frequency components at ω_o and $\omega_o - \omega_s$, and two pairs of microwave signal modulation sidebands at $\omega_o \pm \omega_m$ and $\omega_o - \omega_s \pm \omega_m$. The sidebands at $\omega_o - \omega_s \pm \omega_m$ have a phase shift of θ compared to that of $\omega_o \pm \omega_m$. A fibre Bragg grating (FBG) is connected to the output of the PM. It has a reflection spectrum as shown by the blue dotted line in Fig. 2(a). It is used to suppress the frequency components close to the optical carrier. The FBG is followed by a wavelength division multiplexer (WDM). The magnitude responses of Channel 1 and 2 of the WDM are shown by the black and red dashed lines in Fig. 2(b) respectively. The figure shows the upper and lower sidebands can pass through WDM Channel 1 (CH1) and Channel 2 (CH2) respectively. At each WDM channel output, there are two sidebands, which have a frequency difference of ω_s as depicted in Fig. 2(c) and (e). Beating of the two sidebands at a low-frequency photodetector (PD_1 and PD_2) generates an IF signal at ω_s. Fig. 2(d) and (f) depict the IF signals at PD_1 and PD_2 outputs have a phase difference of 2θ, which is twice the phase difference of the incoming microwave signals received by the two antennas. Since the IF signal frequency is the same as the frequency of the ramp waveform into the DP-MZM and the frequency of the ramp can be few tens of kHz, the two output IF signal phase difference can be measured using a low-frequency low-cost electronic phase detector. The incoming microwave signal phase difference and consequently

the microwave signal AOA can be obtained according to the IF signal phase difference.

III. Analysis and Discussion

Referring to Fig. 1, the continuous wave light generated by the laser diode is intensity modulated by the microwave signal received by Antenna 1, and MZM_A and MZM_B are biased at the MITP and MATP respectively. The electric field at the DP-MZM output is given by

$$E_{o,DPMZM}(t) = \frac{1}{2}E_{in}\sqrt{t_{ff_1}}e^{j\omega_o t}\left[-J_1(m_{RF1})e^{-j\omega_m t} + e^{-j\omega_s t} + J_1(m_{RF1})e^{j\omega_m t}\right] \quad (2)$$

where E_{in} is the DP-MZM input continuous wave light electric field amplitude, t_{ff1} is the DP-MZM insertion loss, $J_n(m)$ is the Bessel function of the first kind of order n, $m_{RF1} = \pi V_{RF1}/V_{\pi,MZM}$ is the modulation index of the intensity modulated optical signal produced by MZM_A, V_{RF1} is the voltage of the microwave signal received by Antenna 1 and $V_{\pi,MZM}$ is MZM_A RF port half wave voltage. The frequency components at ω_o-ω_m, $\omega_o-\omega_s$, and $\omega_o+\omega_m$ shown in (2) are phase modulated by the microwave signal received by Antenna 2. The electric field at the PM output can be expressed as

$$\begin{aligned} E_{o,PM}(t) = {} & \frac{1}{2}E_{in}\sqrt{t_{ff_1}t_{ff2}}e^{j\omega_o t} \\ & \times \left[-J_1(m_{RF1})e^{-j(\omega_m t-\omega_m T)} + e^{-j(\omega_s t-\omega_s T)} \right. \\ & \left. +J_1(m_{RF1})e^{j(\omega_m t-\omega_m T)}\right] \\ & \times \left[J_0(m_{RF2}) + J_1(m_{RF2})e^{j(\omega_m t+\theta)} \right. \\ & -J_1(m_{RF2})e^{-j(\omega_m t+\theta)} + J_2(m_{RF2})e^{j(2\omega_m t+2\theta)} \\ & \left. +J_2(m_{RF2})e^{-j(2\omega_m t+2\theta)}\right] \end{aligned} \quad (3)$$

where t_{ff2} is the PM insertion loss, T is the time delay for the optical signal travelled from the DP-MZM to the PM, $m_{RF2} = \pi V_{RF2}/V_{\pi,PM}$ is the modulation index of the phase modulated optical signal produced by the PM, V_{RF2} is the voltage of the microwave signal received by Antenna 2 and $V_{\pi,PM}$ is the PM half wave voltage. The PM output optical signal passes through the FBG and the WDM, which suppress the optical carrier and the unwanted sidebands. WDM CH1 and CH2 output optical spectrums are depicted in Fig. 3(a) and (b) respectively. Compared to Fig. 2(c) and (e), Fig. 3 shows WDM CH1 and CH2 output consists of the unwanted 1st order sidebands, the residual optical carriers and the 2nd order sidebands, in addition to the wanted 1st order sidebands. The lower and upper 2nd order sidebands are far away from WDM CH1 and CH2 passband respectively. Hence, they are largely suppressed by the WDM and are not shown in Fig. 3(a) and (b).

The two WDM channel output electric fields can be obtained from (3). They are given by

$$\begin{aligned} E_{o,CH1}(t) = {} & \frac{1}{2}E_{in}\sqrt{t_{ff_1}t_{ff_2}}e^{j\omega_o t} \\ & \times \left[-\sqrt{\alpha_2(\omega_o-\omega_m)}A_{-1}e^{-j\omega_m t} + \sqrt{\alpha_1}A_0 \right. \\ & \left. +A_1e^{j\omega_m t} + A_2e^{j2\omega_m t}\right] \end{aligned} \quad (4)$$

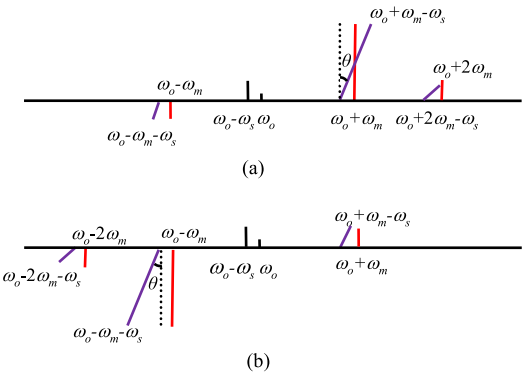

Fig. 3. WDM (a) CH1 and (b) CH2 output optical spectrum.

$$\begin{aligned} E_{o,CH2}(t) = {} & \frac{1}{2}E_{in}\sqrt{t_{ff_1}t_{ff_2}}e^{j\omega_o t} \\ & \times \left[-A_{-2}e^{-j2\omega_m t} - A_{-1}e^{-j\omega_m t} + \sqrt{\alpha_1}A_0 \right. \\ & \left. +\sqrt{\alpha_2(\omega_o+\omega_m)}A_1e^{j\omega_m t}\right] \end{aligned} \quad (5)$$

where α_1 represents the amount of suppression at around the optical carrier frequency introduced by the FBG, $\alpha_2(\omega_o$-$\omega_m)$ and $\alpha_2(\omega_o+\omega_m)$ represent the amount of suppression at the lower and upper 1st order sideband introduced by WDM CH1 and CH2 respectively, A_0, $A_{\pm1}$ and $A_{\pm2}$ are the amplitude coefficients of the optical carrier, the lower and upper 1st order sideband, and the lower and upper 2nd order sideband respectively, which are given by

$$\begin{aligned} A_0 = {} & \left[J_0(m_{RF2})e^{-j(\omega_s t-\omega_s T)} \right. \\ & \left. -2J_1(m_{RF1})J_1(m_{RF2})\cos(\theta+\omega_m T)\right] \end{aligned} \quad (6)$$

$$\begin{aligned} A_{\pm1} = {} & \left[J_1(m_{RF2})e^{\pm j\theta}e^{-j(\omega_s t-\omega_s T)} \right. \\ & +J_0(m_{RF2})J_1(m_{RF1})e^{\mp j(\omega_m T)} \\ & \left. -J_1(m_{RF1})J_2(m_{RF2})e^{\pm j(\omega_m T+2\theta)}\right] \end{aligned} \quad (7)$$

$$\begin{aligned} A_{\pm2} = {} & \left[J_2(m_{RF2})e^{\pm j2\theta}e^{-j(\omega_s t-\omega_s T)} \right. \\ & \left. +J_1(m_{RF1})J_1(m_{RF2})e^{\pm j(-\omega_m T+\theta)}\right] \end{aligned} \quad (8)$$

For simplicity, we assume $\alpha_2(\omega_o$-$\omega_m) = \alpha_2(\omega_o+\omega_m) = \alpha_2(\omega_o\pm\omega_m)$. The photocurrent at the IF signal angular frequency ω_s at the output of PD_1 and PD_2 can be found from (4) and (5). They are given by

$$\begin{aligned} I_{PD1} = {} & \frac{1}{2}P_{in}\Re t_{ff_1}t_{ff_2}J_1(m_{RF1})J_1(m_{RF2}) \\ & \sqrt{{C_1}^2+{C_2}^2}\cos\left(\omega_s t-\omega_s T+{}^{\beta}/_{2}\right) \end{aligned} \quad (9)$$

$$I_{PD2} = \frac{1}{2} P_{in} \Re t_{ff_1} t_{ff_2} J_1(m_{RF1}) J_1(m_{RF2}) \sqrt{{C_1}^2 + {C_2}^2} \cos\left(\omega_s t - \omega_s T - {}^{\beta}/_{2}\right) \quad (10)$$

where P_{in} is the DP-MZM input continuous wave light power, $\Re$ is the responsivity of the photodetector, and

$$C_1 = [-J_2(m_{RF2})\alpha_2(\omega_o \pm \omega_m) + J_0(m_{RF2})(\alpha_2(\omega_o \pm \omega_m) + 1) - 2\alpha_1 J_0(m_{RF2})] \times \cos(\omega_m T + \theta) \quad (11)$$

$$C_2 = [J_2(m_{RF2})(\alpha_2(\omega_o \pm \omega_m) - 2) + J_0(m_{RF2})(\alpha_2(\omega_o \pm \omega_m) - 1)] \sin(\omega_m T + \theta) \quad (12)$$

$$\beta = 2tan^{-1}\left(\tan(-\omega_m T - \theta)\left[\frac{C_2}{C_1}\right]\right) \quad (13)$$

(9) and (10) show the two output IF signals have the same amplitude. They also show the two output IF signal phase difference is β and is independent to $\omega_s T$. Under an ideal situation, the unwanted 1st order sidebands and the residual optical carriers are eliminated by the WDM and the FBG, i.e., α_1 and $\alpha_2(\omega_o \pm \omega_m)$ are equal to 0, and for a small input microwave signal, the 2nd order sidebands have small amplitudes and can be ignored. In this case, C_2/C_1 becomes -1. For an incoming microwave signal angular frequency that results in $\omega_m T$ to be an integer multiple of π, the IF signal phase difference β becomes twice the incoming microwave signal phase difference 2θ as was discussed in Section II. For the case where $\omega_m T$ is not an integer multiple of π, the incoming microwave signal phase difference can be obtained using (13) together with the system output IF signal phase difference and the incoming microwave signal angular frequency ω_m. As with most reported AOA measurement systems, the incoming microwave signal angular frequency needs to be known in order for the proposed structure to determine the microwave signal AOA.

According to (1), when the two antennas have a half wavelength separation, the estimated microwave signal AOA becomes $\varphi = \sin^{-1}(\theta/\pi)$. Since the IF signal phase difference is $\beta = 2\theta$, the microwave signal AOA can be obtained from the IF signal phase difference i.e., $\varphi = \sin^{-1}(\beta/2\pi)$. Hence, the estimated microwave signal AOA can be written as

$$\varphi = \sin^{-1}\left(\frac{\tan^{-1}\left[-\tan(\theta)\frac{C_1}{C_2}\right]}{\pi}\right) \quad (14)$$

(14) shows the present of the residual optical carriers and the unwanted 1st and 2nd order sidebands cause the estimated AOA to deviate from the actual AOA of $\sin^{-1}(\theta/\pi)$. Fig. 4(a) shows the difference between the estimated AOA and the actual AOA for different amounts of unwanted 1st order sideband suppression $\alpha_2(\omega_o \pm \omega_m)$. A carrier suppression of 35 dB, i.e., $\alpha_1 = -35$ dB, was used in the simulation, which can be achieved by using a dense wavelength division multiplexing (DWDM) FBG [18]. As shown in Fig. 4(a), the unwanted 1st order sidebands need to be suppressed by more than 15 dB to ensure less than 1° difference between the estimated and actual AOAs. (14) also shows the

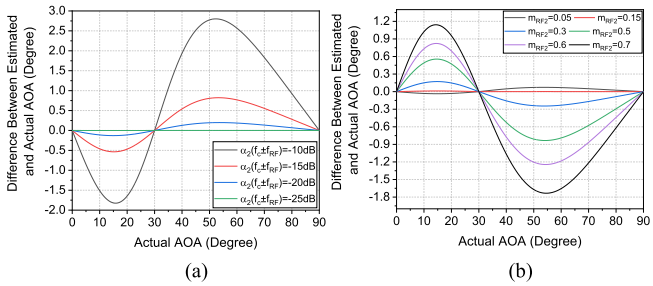

Fig. 4. Simulated difference between the estimated and actual AOA versus the actual AOA for (a) different amounts of unwanted 1st order sideband suppression while $m_{RF2} = 0.15$, and (b) different phase modulated optical signal modulation indexes while $\alpha_2(\omega_o \pm \omega_m) = -25$ dB.

estimated AOA is dependent on the phase modulated optical signal modulation index m_{RF2}. Fig. 4(b) shows the difference between the estimated AOA and the actual AOA for different modulation indexes m_{RF2}. It can be seen from the figure that the modulation index that results in the smallest difference between the estimated and actual AOA is 0.15. For $m_{RF2}<0.15$, the 1st order sidebands have small amplitude and hence the residual carriers have more effect on the output IF signal phase difference. This causes the estimated AOA to be different from the actual AOA. For $m_{RF2}>0.15$, the effect of the 2nd order sidebands on the output IF signal phase difference increases, which increases the difference between the estimated and actual AOA. The estimated and actual AOA difference is within $\pm 1°$ when the modulation index is less than 0.5. Note from Fig. 4 that the difference between the estimated and actual AOA is maximum when the actual AOA is 54.5°.

A digital phase detector (DPD) based on a field-programmable gate array (FPGA) can be used to measure $0°-360°$ phase difference of the two low-frequency IF signals [19], [20]. Since the phase difference of the IF signal is twice the phase difference of the microwave signal received by two antennas and a DPD can detect a phase difference of 0° to 360°, a microwave signal phase difference of 0° to 180° can be detected. This corresponds to a 0°-90° AOA measurement range. A DPD can be designed to have a high resolution of 1°. Hence, using a DPD to measure the phase difference of the two output IF signals in the proposed structure, a microwave signal phase difference with a resolution of 0.5° can be determined. The phase detection performance of a DPD is not affected by change in the input signal power. Hence changing the power of the microwave signal received by the antennas, which alters the photodetector output IF signal power, has no effect on the AOA measurement. This solves the incoming microwave signal power dependent AOA measurement problem in the reported AOA measurement systems [5]–[8]. A DPD is compact and low cost compared to an ESA or an oscilloscope used in the reported AOA measurement systems [9]–[11], [13].

The proposed AOA measurement system does not require any high-frequency electrical component. Its upper operating frequency is limited by the optical modulator bandwidth. DP-MZMs with over 40 GHz bandwidth and low insertion loss of below 4 dB are commercially available. The lower operating

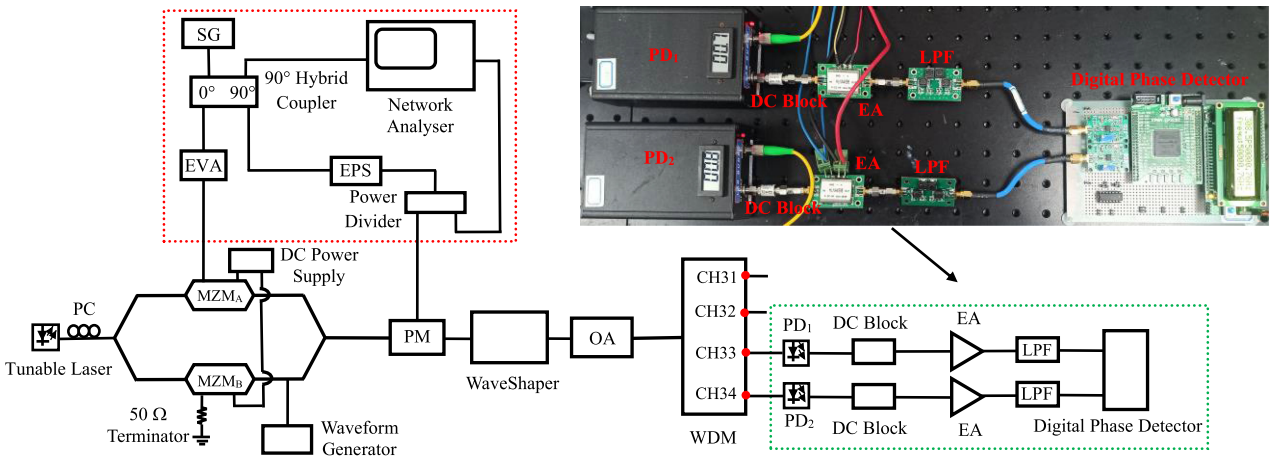

Fig. 5. Frequency converter based AOA measurement system experimental setup. PC: polarisation controller; EVA: electrical variable attenuator; SG: signal generator; EPS: electrical phase shifter; OA: Optical amplifier; EA: electrical amplifier; LPF: lowpass filter. Inset is the photo of the experimental setup showing the components inside the green dotted box.

frequency of the proposed AOA measurement system is determined by the 3 dB reflection spectrum width of the FBG used for suppressing the optical carrier. A DWDM FBG with a narrow 12.5 GHz 3 dB reflection spectrum width and over 35 dB stopband rejection [18] can be employed in the frequency converter based AOA measurement system to largely suppress the optical carrier while passing the microwave signal modulation sideband of around 6 GHz away from the optical carrier. The edge roll-off of a standard WDM magnitude response is around 100 dB/nm. This limits the amount of unwanted 1st order sideband suppression to less than 8 dB for an input microwave signal with a frequency below 10 GHz. This causes large difference between the estimated and actual AOAs as shown in Fig. 4(a). In order to ensure the proposed system can operate at low frequencies of, for example, 6 GHz with small AOA measurement errors, several low-cost thin film optical filters with the same centre frequency as the WDM channel frequency can be connected at the WDM channel output to increase the sharpness of the overall magnitude response edge. It has been demonstrated in [21] that a 403 dB/nm edge roll-off bandpass filter magnitude response can be realised by cascading three low-cost thin film optical filters. Hence the frequency converter based AOA measurement system can be operated from 6 to 40 GHz using commercial off-the-shelf components.

IV. Experimental Results

Fig. 5 shows the experimental setup to demonstrate the proposed AOA measurement system. A tunable laser was used as an optical source (Keysight N7711A). It generated a 15.6 dBm continuous wave light, which passed through a polarisation controller (PC), into a Sumitomo 20 GHz bandwidth DP-MZM. A network analyser (Keysight E5063A), a microwave signal generator (Hittite HMC-T2220) and various electrical components inside the red dotted box in Fig. 5 were used to generate two microwave signals with an adjustable phase difference. They are not required in the actual AOA measurement system. A 15 GHz microwave signal from the microwave signal generator was equally spilt into two via a 90° hybrid coupler. The two microwave signals passed through an electrical phase shifter (EPS) and an electrical variable attenuator (EVA) before being applied to MZM$_A$ inside the DP-MZM and an EOSpace 20 GHz bandwidth PM connected to the DP-MZM output. The EVA and the EPS were used to control the amplitude and the phase difference of the two microwave signals respectively. The network analyser was used to measure the phase difference of the microwave signals into the DP-MZM and the PM. MZM$_B$ RF port was connected to a 50 Ω terminator. A waveform generator (Rigol DG4102), which generated a 50 kHz ramp waveform, was connected to the DC port of the main MZM in the DP-MZM. The amplitude of the ramp waveform was set to be two times the half wave voltage of the main MZM, which is 5.95 V, to shift the frequency of the optical carrier travelled in the bottom path of the main MZM and to ensure the spurious components generated by the frequency shifting process are more than 30 dB below the frequency shifted optical carrier. A dual-output power supply was employed to set MZM$_A$ and MZM$_B$ bias points at the MITP and MATP respectively. As an FBG was not available, the optical carrier was suppressed by a WaveShaper (Finisar WS-04000A), which was programmed to have a notch filter magnitude response with the notch frequency at around the optical carrier frequency. The WaveShaper was followed by an optical amplifier (OA) to amplify the optical signal power to 11 dBm before launching into a four-channel WDM. The wavelength of the continuous wave light from the tunable laser was adjusted to 1550.72 nm so that the optical carrier was located at the midpoint of WDM CH33 and CH34.

The PM and the OA output optical spectrums are shown in Fig. 6(a) and (b) respectively. The figures also show the normalised notch filter magnitude response produced by the WaveShaper, and the normalised magnitude responses of WDM CH33 and CH34. As shown in Fig. 6(b), WDM CH33 magnitude response has a gradual edge roll-off compared to WDM

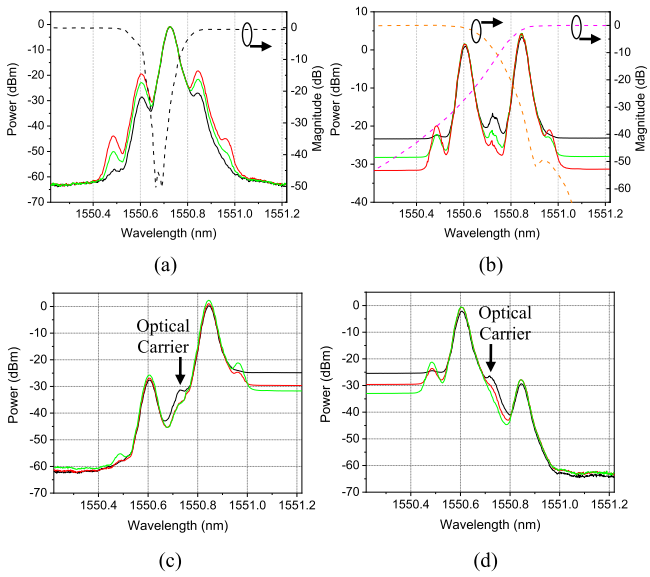

Fig. 6. Optical spectrums measured at the output of (a) the PM, (b) the OA, (c) WDM CH33 and (d) WDM CH34 for 0.2 (black), 0.4 (green) and 0.6 (red) modulation index. Magnitude responses of the WaveShaper (black dashed line), WDM CH33 (pink dashed line) and WDM CH34 (orange dashed line).

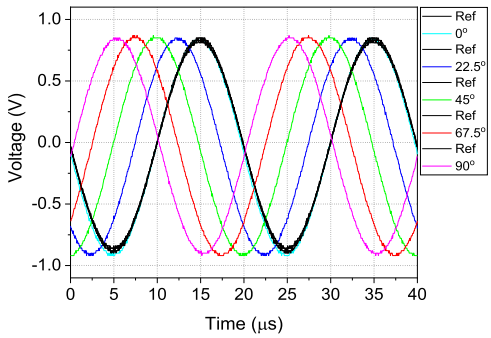

Fig. 7. Measured IF signal waveforms at the output of PD_1 (black) and PD_2 when the two input microwave signals have 0° (cyan), 22.5° (blue), 45° (green), 67.5° (red) and 90° (pink) phase difference.

CH34. This limits the amount of suppression in the lower 1st order sidebands at WDM CH33 output. In order to obtain large unwanted 1st order sideband suppression at both WDM CH33 and CH34 outputs, the WaveShaper magnitude response was programmed to make the frequency of the notch slightly away from the optical carrier as shown in Fig. 6(a). Fig. 6(c) and (d) show the residual carriers at WDM CH33 and CH34 output are more than 31.5 dB and 24.5 dB below the wanted 1st order sideband respectively for a modulation index of more than 0.2. The figures also show, for a 15 GHz microwave signal into the modulators, the unwanted 1st order sidebands at WDM CH33 and CH34 outputs have almost the same amount of suppression by the WaveShaper and the WDM, which are 27.8 dB and 27.4 dB respectively. As shown in Fig. 6(c) and (d), the amplitude of the 2nd order sideband on the same side of the wanted 1st order sideband is higher than the unwanted 1st order sideband and residual carrier amplitudes. Thus, this is the main factor

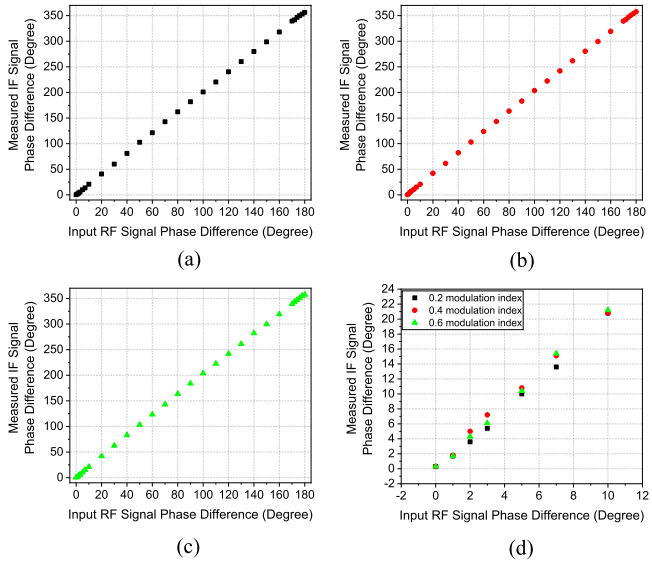

Fig. 8. Measured IF signal phase difference versus the phase difference of the input microwave signal for (a) 0.2, (b) 0.4 and (c) 0.6 modulation index. (d) IF signal phase difference measurement in a 0° to 10° input microwave signal phase difference range.

that causes the IF signal phase difference to deviate from twice the input microwave signal phase difference. Nevertheless, its effect on the IF signal phase difference is small as it is over 20 dB below the wanted 1st order sideband for a modulation index of less than 0.6.

The optical signals at WDM CH33 and CH34 outputs were detected by two photodetectors, which generated two IF signals at 50 kHz. The two output IF signal waveforms, when a 15 GHz microwave signal into the modulators, were measured on a four-channel 100 MHz bandwidth oscilloscope (Keysight DSO-X2014A). Fig. 7 shows the IF signal waveform measured at PD_1 output (black line), which is referred to as a reference (Ref) waveform, remains unchanged, but the phase of the IF signal waveform measured at the output of PD_2 changes, when the EPS is adjusted to alter the input microwave signal phase difference. The coloured lines in Fig. 7 show the waveforms measured at PD_2 output when the input microwave signal phase difference changes from 0° to 90° with a step of 22.5°. The figure reveals the corresponding phase difference of the two output IF signals are 0°, 45°, 90°, 135° and 180°. This verifies the phase difference of the two output IF signals is twice the input microwave signal phase difference.

The output of each photodetector was connected to a DC block, a DC to 1 MHz bandwidth electrical amplifier and a 50 kHz lowpass filter (LPF) as shown inside the green dotted box as well as the photo in the inset of Fig. 5. The two LPF outputs were connected to a FPGA based DPD, which had an LCD display showing the frequency and the phase difference of the two input signals. The DPD used in the experiment can measure the phase difference of the two input signals with amplitudes between 0.1 to 5 V. It has a resolution of 0.1°. The EPS at the PM input was adjusted to introduce a phase difference between the microwave signal into the two modulators. Fig. 8(a) illustrates

TABLE I
COMPARISON BETWEEN THE REPORTED AND PROPOSED AOA MEASUREMENT SYSTEMS

	Configuration	No High-Frequency Electrical Component	Suitable For Long Baseline System	Input RF Signal Amplitude Independent	Measuring Instrument
[5]	Two Cascaded MZMs	✓	✓	×	Optical Power Meter
[6]	DD-MZM	✓	×	×	Optical Power Meter
[7]	Two Cascaded MZMs	✓	✓	×	RF Power Meter
[8]	DD-MZM	✓	×	×	Digital Multimeter
[9]	Two Parallel Connected MZMs	✓	✓	✓	ESA
[10]	DPol-MZM	✓	×	✓	ESA
[11]	DD-MZM	×	×	✓	Oscilloscope
[12]	DP-MZM	✓	×	×	Optical Power Meter
[13]	DP-MZM and MZM Connected in Parallel	×	×	✓	Low-Frequency ESA
Current work	Cascaded DP-MZM and PM	✓	✓	✓	DPD

DD-MZM: Dual-Drive MZM; DPol-MZM: Dual-Polarisation MZM; DP-MZM: Dual-Parallel MZM; PM: Phase Modulator.

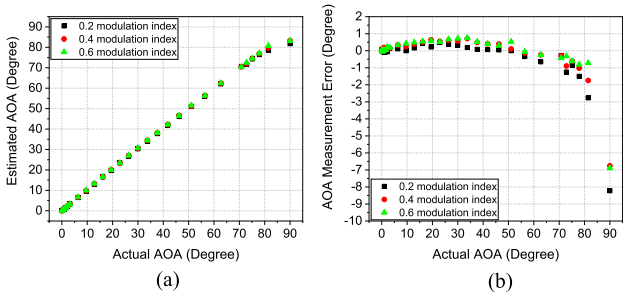

Fig. 9. (a) Estimated AOA versus actual AOA for 0.2, 0.4 and 0.6 microwave signal modulation indexes, and (b) the corresponding AOA measurement errors.

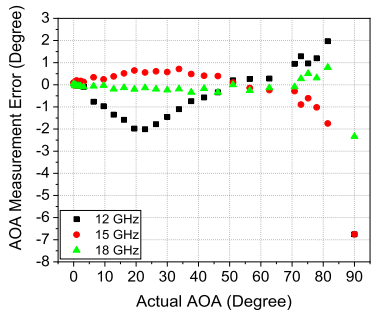

Fig. 10. AOA measurement error versus actual AOA for different frequency microwave signals into the AOA measurement system.

the IF signal phase difference measured on the DPD is twice the phase difference of the input microwave signal. Fig. 8(d) shows the IF signal phase difference is changed by around 2° for every 1° microwave signal phase difference change. A 1° change in the microwave signal phase difference in a 0°−10° microwave signal phase difference range corresponds to <0.4° change in the microwave signal AOA. This indicates that the proposed structure has high resolution microwave signal AOA measurement capability. Fig. 8(b) and (c) show the IF signal phase difference measurement when the modulation index was increased to 0.4 and 0.6 respectively. As shown in the figures, the relationship of $\beta = 2\theta$ holds for different modulation indexes, which demonstrates the important advantage of input microwave signal power independent AOA measurement performance.

The measured IF signal phase differences shown in Fig. 8 were used to obtain the estimated AOAs, which are depicted in Fig. 9(a). The AOA measurement error, which is the difference between the estimated and actual AOA, is depicted in Fig. 9(b). The figure shows the proposed structure can determine the microwave signal AOA with errors within −2.7° to 1° in a 0° to 81.5° AOA measurement range for 0.2, 0.4 and 0.6 modulation indexes. Large AOA measurement errors for a microwave signal AOA close to 90° is because the microwave signal AOA φ and the microwave signal phase difference θ has a relationship of $\varphi = \sin^{-1}(\theta/\pi)$. Therefore, changing a microwave signal phase difference from 179° to 180° results in an AOA changes from 84° to 90°. Hence, a small measurement error for an IF signal phase difference of around 360° will lead to a large AOA measurement error. Note that several reported AOA measurement systems show the ability of measuring microwave signal AOA with errors of less than ±2° [7], [8], [13]. However, the small AOA measurement errors are obtained in a small AOA measurement range, these AOA measurement systems cannot be used in a long baseline interferometer antenna system, and/or an expensive and bulky ESA is needed to measure the microwave signal AOA. To show the frequency converter based AOA measurement system is capable to operate at various input microwave signal frequencies, the IF signal phase difference measurement shown in Fig. 8 was repeated for a 12 GHz and 18 GHz input microwave signal frequency while the microwave signal modulation index was kept at 0.4. Fig. 10 shows the AOA measurement errors obtained from the measured IF signal phase differences. The figure reveals that, for different input microwave signal frequencies, the AOA measurement errors remain below ±2° in a 0° to 81.5° AOA measurement range. A comparison between the reported and proposed AOA measurement systems is shown in Table I. This shows the proposed AOA measurement system has the advantages of not requiring high-frequency electrical component, suitable for use in a long baseline interferometer antenna system, using low-cost low-frequency DPD for AOA measurement, and having an input microwave signal power independent AOA measurement capability.

V. CONCLUSION

A frequency converter based AOA measurement system has been presented. The system is based on down converting a high-frequency microwave signal received by two antennas into

two low-frequency IF signals. Using a low-frequency low-cost DPD to measure the phase difference of the system output IF signals, the incoming microwave signal phase difference and consequently the AOA can be determined. Instead of using a traditional high-frequency tunable LO source, a fixed low-frequency ramp waveform is used for the frequency conversion process. No high-frequency electrical component is needed and hence the proposed structure has a wide operating frequency range. The effect of the residual carrier and the unwanted 1st and 2nd order sidebands on the AOA measurement system performance have been investigated. An experiment has been set up to measure the phase difference of two IF signals at the output of the proposed frequency converter based AOA measurement system. Results demonstrate the microwave signal AOA can be accurately measured with less than $\pm 3^\circ$ measurement errors in an AOA measurement range of $0^\circ - 81.5^\circ$, for different frequency and different power input microwave signals.

REFERENCES

[1] S. Pan and J. Yao, "Photonics-based broadband microwave measurement," *J. Lightw. Technol.*, vol. 35, no. 16, pp. 3498–3513, Aug. 2017.

[2] A. H. Sayed, A. Tarighat, and N. Khajehnouri, "Network-based wireless location: Challenges faced in developing techniques for accurate wireless location information," *IEEE Signal Process. Mag.*, vol. 22, no. 4, pp. 24–40, Jul. 2005.

[3] D. Niculescu and B. Nath, "Ad hoc positioning system (APS) using AOA," in *Proc. 22nd Annu. Joint Conf. IEEE Comput. Commun. Societies*, vol. 3, 2003, pp. 1734–1743.

[4] M. E. Manka, "Microwave photonics for electronic warfare applications," in *Proc. IEEE Int. Topical Meeting Microw. Photon.*, 2008, pp. 275–278.

[5] X. Zou, W. Li, W. Pan, B. Luo, L. Yan, and J. Yao, "Photonic approach to the measurement of time-difference-of-arrival and angle-of-arrival of a microwave signal," *Opt. Lett.*, vol. 37, no. 4, pp. 755–757, Feb. 2012.

[6] Z. Cao, Q. Wang, R. Lu, H. P. A. van den Boom, E. Tangdiongga, and A. M. J. Koonen, "Phase modulation parallel optical delay detector for microwave angle-of-arrival measurement with accuracy monitored," *Opt. Lett.*, vol. 39, no. 6, pp. 1497–1500, 2014.

[7] H. Chen and E. H. W. Chan, "Angle of arrival measurement system using double RF modulation technique," *IEEE Photon. J.*, vol. 11, no. 1, Feb. 2019, Art. no. 7200110.

[8] H. Chen and E. H. W. Chan, "Simple approach to measure angle of arrival of a microwave signal," *IEEE Photon. Technol. Lett.*, vol. 31, no. 22, pp. 1795–1798, Nov. 2019.

[9] B. Vidal, M. A. Piqueras, and J. Marti, "Direction-of-arrival estimation of broad microwave signals in phased-array antennas using photonic techniques," *J. Lightw. Technol.*, vol. 24, no. 7, pp. 2741–2745, Aug. 2006.

[10] Z. Tu, A. Wen, Z. Xiu, W. Zhang, and M. Chen, "Angle-of-arrival estimation of broadband microwave signals based on microwave photonic filtering," *IEEE Photon. J.*, vol. 9, no. 5, Oct. 2017, Art. no. 5503208.

[11] P. Li *et al.*, "Angle-of-arrival estimation of microwave signals based on optical phase scanning," *J. Lightw. Technol.*, vol. 37, no. 24, pp. 6048–6053, Dec. 2019.

[12] H. Zhuo, A. Wen, and Y. Wang, "Photonic angle-of-arrival measurement without direction ambiguity based on a dual-parallel Mach–Zehnder modulator," *Opt. Commun.*, vol. 451, pp. 286–298, 2019.

[13] H. Chen, C. Huang, and E. H. W. Chan, "Photonic approach for measuring AOA of multiple signals with improved measurement accuracy," *IEEE Photon. J.*, vol. 12, no. 3, Jun. 2020, Art. no. 7201810.

[14] J. Kolanek and E. Carlsen, "Precision geolocation system and method using a long baseline interferometer antenna system," U.S. Patent 7286085, 2007.

[15] P. D. Biernacki, R. Madara, L. T. Nichols, A. Ward, and P. J. Matthews, "A four channel angle of arrival detector using optical downconversion," in *Proc. IEEE MTT-S Int. Microw. Symp. Dig.*, vol. 3, 1999, pp. 885–888.

[16] L. M. Johnson and C. H. Cox, "Serrodyne optical frequency translation with high sideband suppression," *J. Lightw. Technol.*, vol. 6, no. 1, pp. 109–112, Jan. 1988.

[17] C. Huang and E. H. W. Chan, "Photonics-based serrodyne microwave frequency translator with large spurious suppression and phase shifting capability," *J. Lightw. Technol.*, vol. 39, no. 7, pp. 2052–2058, Apr. 2021.

[18] O/E Land DWDM fiber Bragg gratings (OEWDM-012) data sheet. [Online]. Available: http://www.o-eland.com/FiberGratingProducts/FiberGrating_wdm_product.php

[19] S. J. Lu, P. Siqueira, V. Vijayendra, H. Chandrikakutty, and R. Tessier, "Real-time differential signal phase estimation for space-based systems using FPGAs," *IEEE Trans. Aerosp. Electron. Syst.*, vol. 49, no. 2, pp. 1192–1209, Apr. 2013.

[20] J. Mitra and T. K. Nayak, "An FPGA-based phase measurement system," *IEEE Trans. Very Large Scale Integration Syst.*, vol. 26, no. 1, pp. 133–142, Jan. 2018.

[21] C. Huang, E. H. W. Chan, and C. B. Albert, "A compact photonics-based single sideband mixer without using high-frequency electrical components," *IEEE Photon. J.*, vol. 11, no. 4, Aug. 2019, Art. no. 7204509.